2424 *Biochemistry* **2010,** *49,* 2424–2432
DOI: 10.1021/bi902140e

BIOCHEMISTRY
including biophysical chemistry & molecular biology
Article

Dependence of Catalytic Activity on Driving Force in Solution Assays and Protein Film Voltammetry: Insights from the Comparison of Nitrate Reductase Mutants[†]

Vincent Fourmond,[‡] Bénédicte Burlat,[‡] Sébastien Dementin,[‡] Monique Sabaty,[§] Pascal Arnoux,[§] Émilien Étienne,[‡] Bruno Guigliarelli,[‡] Patrick Bertrand,[‡] David Pignol,[§] and Christophe Léger*[,‡]

[‡]*Centre National de la Recherche Scientifique, UPR 9036, Unité de Bioénergétique et Ingénierie des Protéines, Institut de Microbiologie de la Méditerranée, and Aix-Marseille Université, 31 chemin Joseph Aiguier, 13402 Marseille Cedex 20, France, and* [§]*Laboratoire de Bioénergétique Cellulaire, Commissariat à l'Energie Atomique, DSV, IBEB, 13108 Saint-Paul-lez-Durance, France, and Centre National de la Recherche Scientifique, UMR 6191, Biologie Végétale et Microbiologie Environnementale, and Aix-Marseille Université, 13108 Saint-Paul-lez-Durance, France*

Received December 14, 2009; Revised Manuscript Received February 2, 2010

ABSTRACT: *Rhodobacter sphaeroides* periplasmic nitrate reductase (*Rs* NapAB) is one of the enzymes whose assays give odd results: in spectrophotometric assays with methyl viologen as the electron donor, the activity increases as the reaction progresses, whereas the driving force provided by the soluble redox partner decreases; in protein film voltammetry (PFV), whereby the enzyme directly exchanges electrons with an electrode, the activity of NapAB decreases at large overpotential, whereas a monotonic increase is expected [Elliott, S. J., et al. (2002) *Biochim. Biophys. Acta 1555*, 54−59]. The relations between these phenomena and the catalytic mechanism are still debated. By studying NapAB mutants, we found that the peculiar dependences of electrochemical and solution activities on driving force are greatly affected by substituting certain amino acids that are located in the vicinity of the active site (M153, Q384, R392); this led us to establish and discuss the relation between the experimental parameters of the electrochemical and spectrophotometric assays: we show that the rate of reduction of the enzyme (which depends on the electrode potential or on the concentration of reduced MV) modulates the activity of the enzyme, but the "solution potential" does not. Our results also support the view that the complex profiles of activity versus potential are fingerprints of the active site chemistry, rather than direct consequences of changes in the redox states of relays that are remote from the active site.

Multicenter redox enzymes usually follow a ping-pong mechanism whereby a substrate is reduced or oxidized at a catalytic site and electrons come from, or are transferred to, a remote site where the redox partner is oxidized or reduced, respectively. Here we shall consider the common situation where this remote site is an electron transfer center, like a heme or an iron−sulfur cluster, which can interact unspecifically with artificial redox dyes. In that case, the activity is conveniently assayed by following the change in absorbance of the solution as a function of time. Alternatively, if the enzyme can be adsorbed onto an electrode in a configuration such that electrons can be directly transferred to or from the remote center, the activity can be simply measured as a catalytic current; this technique is called protein film voltammetry (PFV[1] (*1*), or "protein film electrochemistry" (*2*), or simply "direct electrochemistry" (*3*)).

A major advantage of the electrochemical approach is that the thermodynamic driving force for the catalytic reaction can be continuously varied by adjusting the electrode potential, while the corresponding steady-state activity is simultaneously measured as a current. In a common electrochemical experiment, the electrode potential is swept up and down, and the plot of current against potential (the "cyclic voltammogram") portrays the change in activity against driving force (positive current = oxidation, negative current = reduction). In contrast, in solution assays, one prefers to measure initial rates under conditions where the concentration of the redox dye is saturating and, ideally, constant. The driving force is somehow related to the concentration and reduction potential of the redox partner, but the effect of changing this parameter is seldom examined. Reference *4* is a rare example where the initial rate of hydrogen production by NiFe hydrogenase was measured as a function of the "redox potential" or "solution potential".[2]

The relation between activity and driving force matters because PFV experiments have shown that, in many cases, the highest activity is not obtained at the greatest driving force; instead, it appears to be optimized in a certain potential window, and this may have physiological relevance (*5*). We illustrate this in Figure 1A by showing a typical catalytic voltammogram obtained with *Rhodobacter sphaeroides* (*Rs*) periplasmic nitrate reductase (NapAB). NapAB is a member of the DMSO reductase family of mononuclear molybdoenzymes. These enzymes share a common Mo−bis(molybdopterin) cofactor (Moco) and specifically catalyze the oxidation or reduction of various small

[†]This work is funded by the CNRS, CEA, ANR, Aix-Marseille Université, and the City of Marseilles.

*Corresponding author: e-mail, christophe.leger@ifr88.cnrs-mrs.fr; tel, +33 4 91 16 45 29; fax, +33 4 91 16 40 97.

[1]Abbreviations: *A*, absorbance; DT, dithionite; Moco, molybdenum cofactor; MV, methyl viologen; Nap, periplasmic nitrate reductase; PFV, protein film voltammetry; SHE, standard hydrogen electrode; *Rs*, *Rhodobacter sphaeroides*.

[2]We use quotation marks here because the "solution potential" actually refers to the potential of an electrode that contacts the solution; it is not the electric potential of the solution.

 Published on Web 02/10/2010

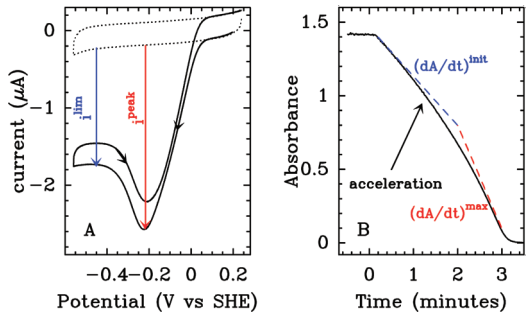

FIGURE 1: Typical results for the electrochemical (A) and spectrophotometric (B) assays of nitrate reduction by *Rs* periplasmic NapAB. In (A), the enzyme is adsorbed onto an electrode which substitutes for the soluble redox partner. The electrode potential is swept forward and backward, as indicated by the black arrows. The dotted line is a blank recorded in the absence of nitrate. The more negative the current, the greater the activity (pH 7.7, 25 °C, 0.27 mM nitrate; this is well above K_m). The magnitude of the low potential attenuation of the current is characterized by the ratio of peak over limiting currents (i_{peak}/i_{lim}). In (B), the consumption of reduced methyl viologen is monitored at 604 nm. The assay is started by adding the enzyme, and the catalytic rate increases over time. Nitrate is in excess over MVred, and the reaction stops when the latter is exhausted at $t \approx 3$ min (pH 7.5, 25 °C, $[NO_3^-] = 20$ mM; [MV]total = 0.5 mM). For the result of similar experiments with *P. pantotrophus* NapAB, see Figure 5 of ref *10*.

inorganic substrates (*6*, *7*). Figure 1A shows that when the electrode potential is taken down, the reductive activity first increases to a maximum (the current *i* decreases to a minimum) before it drops and eventually plateaus off at high driving force; the same activity profile is observed on the return scan, showing that the response is in the steady state. Such nonmonotonic change in activity against driving force has been observed with NapAB from *R. sphaeroides* (*8*, *9*) and *Paracoccus pantotrophus* (*10*) and various other redox enzymes.[3] The mechanistic implications have not always been clarified.

In the case of NapAB, the behavior in spectrophotometric solution assays with reduced methyl viologen (MVred) as the electron donor is also unexpected: when a large excess of nitrate is reduced by MV, the change in absorbance against time is dominated by a first phase where the activity *increases* over the course of the assay, as the concentration of electron donor decreases and so does the driving force for the reaction (Figure 1B) (*10*).

Among the other members of the DMSO reductase family which have been characterized by PFV, the membrane-bound nitrate and DMSO reductases from *Escherichia coli* also exhibit an optimal potential window for electrocatalytic activity (*19*, *20*), but it has not been possible to detect the acceleration phase in solution assays. No PFV data are available for *Rhodobacter capsulatus* periplasmic DMSO reductase, but with this enzyme, Bray and co-workers did observe that the rate of DMSO reduction in solution assays increases as either benzyl viologen or MV is oxidized (*21*).

Thus, regarding the enzymes of the DMSO reductase family, both phenomena have been observed only in the case of *Rs* (our work) and *P. pantotrophus* (*10*) NapAB. One may therefore wonder whether this is a meaningless coincidence or whether the acceleration in solution assays and the peak in the voltammograms are actually two independent demonstrations that decreasing the driving force for nitrate reduction produces a greater activity. Here, we settle the issue by comparing the kinetic properties of various mutants of periplasmic nitrate reductase, as determined in solution and electrochemical assays. This leads us to discuss the meaning of the term driving force in solution assays and PFV and to establish the relation between the two.

[3]This includes the soluble subcomplexes of bovine (*11*) and *Escherichia coli* complex II (*12*−*14*), a holo form of *Thermus thermophilus* complex II (unpublished results of ours, with the enzyme purified by Sarah O'Kane in the group of Tewik Souliman, Limerik University Ireland), the flavoprotein subcomplex of mitochondrial complex I (*15*), pentaheme nitrite reductases (*16*, *17*), various mononuclear enzymes of the DMSO reductase (*3*), and sulfite oxidase (*18*) families etc.

MATERIALS AND METHODS

The purification of the enzyme was described in refs *22* and *23*. The EPR equipment was described in ref *23*. The electrochemical equipment was described in ref *24*. The enzyme films were prepared using neomycin as coadsorbate and a pyrolytic graphite edge rotating disk electrode (4 mm^2 surface) and then activated by electrochemically reducing the sample as described previously (*25*). Using neomycin greatly increases the film stability. However, we have observed that under certain conditions neomycin on graphite gives peaks that look like noncatalytic signals; control experiments with no protein were used to discard these artifactual signals. The buffer consisted in a mixture of MES, CHES, TAPS, HEPES, and sodium acetate (5 mM each) and 0.1 M NaCl, titrated to the desired pH using concentrated NaOH or HCl. Nitrate was added from stock solutions of potassium nitrate in water (1 mM or 2 M, depending on target concentration). All experiments were performed in a glovebox under an atmosphere of N_2.

Spectrophotometric assays were carried out using a homemade water-jacketed glass open cell (working volume 0.5−1 mL) thermostated using a circulation of water, stirred with a rotating magnet, and located in a glovebox under an atmosphere of N_2. The absorbance was measured using a microprobe (Varian; single arm, 10 mm path length, 3.05 mm diameter, 140 mm length) connected with an optic fiber (Varian; 3 m length) to a UV/visible spectrophotometer (Varian Cary 50). The absorbance was sampled at 10 Hz and averaged over 10 data points. Before the enzyme was added, methyl viologen or methylene blue was reduced by stepwise adding aliquots of a fresh solution of sodium dithionite (DT). The extent of reduction was monitored spectroscopically to ensure that the reaction was complete and that no excess dithionite was left in the reaction buffer.

The data were analyzed with an in-house program called SOAS, available via the Internet at http://bip.cnrs-mrs.fr/bip06 (*26*).

RESULTS

Biochemical and Spectroscopic Characterization of the Mutants. Figure 2A shows the overall structure of *Rs* NapAB (*22*). The large subunit NapA houses a [4Fe4S] cluster and the molybdenum cofactor that characterizes the enzymes of the DMSO reductase family. This iron−sulfur cluster and two *c*-type hemes form an electron transfer chain that connects the active site to the redox partner, which is either a membrane-bound tetraheme NapC under physiological conditions (*27*) or methyl viologen when the activity is assayed using spectrophotometry or the electrode in PFV experiments.

Figure 2B shows the environment of the Moco and the three amino acids which we have mutated. R392 is in the vicinity of the active site, with one of the guanidinium N_η at 9.3 Å from the Mo.

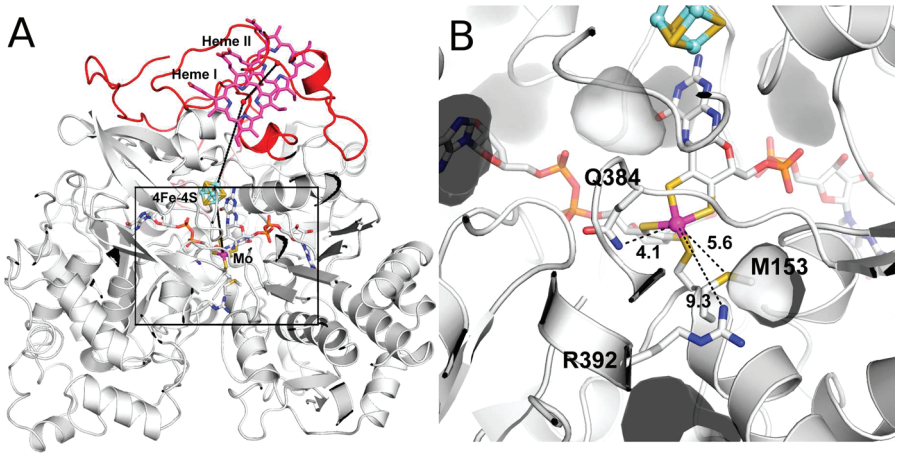

FIGURE 2: Structure of *Rs* NapAB (from PDB 1OGY (*22*)). Panel B is a close-up of the active site.

Replacing R392 with A greatly increases the Michaelis constant for nitrate, suggesting that this residue interacts with the substrate (*23*). The side chain of Q384 is hydrogen bonded to the Mo. We originally replaced Q384 with N in the hope that the mutation would increase the selenate−reductase activity of NapAB (*28*). Decreasing the size of the side chain of the amino acid at position 384 might have favored the binding and/or reduction of selenate, which is bulkier than nitrate, but we found that the mutation has no effect in this respect (unpublished results). M153 is adjacent to C152, which directly ligates the Mo. We described in ref *23* the construction, purification, and kinetic, spectroscopic, and redox properties of the R392A and M153A mutants. We recall the values of certain parameters in Table 1.

Regarding the Q384N mutant, whose characterization has not been published before, metal content analyses confirmed molybdenum incorporation: the molar ratio Fe/Mo, which is equal theoretically to 6, was determined by ICP-MS and found to be 5.6 and 4.9 (±10%) in WT and Q384N, respectively. In the as-prepared states of both enzymes, the two oxidized hemes give at 15 K a single rhombic EPR signal at g = 2.92, 2.28, and 1.50. Upon reduction, this signal disappears progressively, and a rhombic $[4Fe4S]^{+1}$ signal appears at g = 2.042, 1.947, and 1.900 for the WT and g = 2.037, 1.941, and 1.891 for Q384N. Hence the Q384N mutation has no significant effect on the EPR signatures of the hemes and of the [4Fe4S] cluster. The same conclusions were reached in ref *23* for the M153A and R392A variants. Taken together, these results indicate that the mutated enzymes keep their structural integrity and house all cofactors, including the Moco. The redox properties of the [4Fe4S] center were determined in a titration followed by EPR. The Q384N and M153A mutations decrease the reduction potential of the FeS cluster by about 100 mV. The mutants have similar maximal rates (Table 1) despite the fact that the reduction potentials of the [4Fe4S] cluster are different; this demonstrates that electron transfer from the $[4Fe4S]^{+}$ cluster to the Moco does not limit the rate of turnover, at least under the very reducing conditions that prevail when the enzyme is assayed with methyl viologen.

In as-prepared WT *Rs* NapAB, as in periplasmic nitrate reductases from other sources (*25*), the Moco in the +V state gives at 55 K a major "high-g" rhombic signal (g = 1.9989, 1.9908, 1.9812) which exhibits two hyperfine couplings (Figure 3). The interaction with one of the $I = {}^1/_2$ nuclei is resolved only in the g_z component. The hyperfine parameters determined from the simulations are very similar to those published for the Mo(V)

Table 1: Kinetic Parameters of WT and Mutants of *Rs* NapAB Determined from Solution Assays and Reduction Potential of the [4Fe4S] Cluster Determined from Potentiometric Titrations Followed by EPR, As Described in Ref *23*

	V_m[a]	K_m (mM nitrate)[a]	E^0 ([4Fe4S]) (mV vs SHE)	ref
WT *Rs* NapAB	13 ± 1	0.41 ± 0.06	−80 ± 10	*23*
M153A	13 ± 1	3.2 ± 0.7	−180 ± 20	*23*
R392A	12 ± 1	66 ± 6	−100 ± 10	*23*
Q384N	9 ± 1	1.1 ± 0.1	−180 ± 20	this work

[a]The rates are given in μmol of nitrate min^{-1} (mg of protein)$^{-1}$ and measured in the presence of 2 mM reduced MV in 100 mM Tris-HCl buffer at pH 8, 30 °C, from the values of dA/dt at $A \approx 0.5$ (*23*).

high-g signal of *P. pantotrophus* NapAB and attributed to two nonexchangeable protons (*32*). This species is stable over a very large potential range: the midpoint potentials of the Mo(V)/Mo(IV) and Mo(VI)/Mo(V) couples equate −225 and +570 mV, respectively (*22*, *25*). Depending on the enzyme preparation, a minor contribution arising from the so-called "very high g" Mo(V) signal (g = 2.022, 1.999, 1.989) can also be observed. The total spin intensity of the Mo(V) signals represents 0.1−0.2 spin per [4Fe4S] cluster depending on the purification batch. The same signatures (and a similar substoichiometry) are observed in NapAB from *P. pantotrophus* (*25*, *10*). This signal can be detected only as traces in M153A and not at all in R392A (*23*). We have recently demonstrated that it comes from a dead-end species which slowly activates the first time the enzyme is fully reduced (*25*). We did not include the redox properties of the Mo(V) high-g signal in Table 1 because we think that this species is not relevant to the catalytic cycle. We have shown recently that some inactive forms of the Mo *other* than the one giving rise to the high-g signal are reversibly produced when the WT enzyme is exposed to very large concentrations of nitrate (*33*). This manifests as substrate inhibition under mildly reducing conditions and, under certain conditions, as a peculiar hysteresis in the voltammetry. We observed that these effects are very small or nonexistent with the three mutants discussed here.

The as-prepared Q384N mutant also exhibits a Mo(V) signal, which accounts for 0.1 spin per molecule. This signal resembles the high-g signal of the WT enzyme, with only small differences in the g-values, and shows a very similar hyperfine pattern resulting from the coupling with two protons (Figure 3). The additional line at g = 1.985 exhibits the same saturation and redox behavior

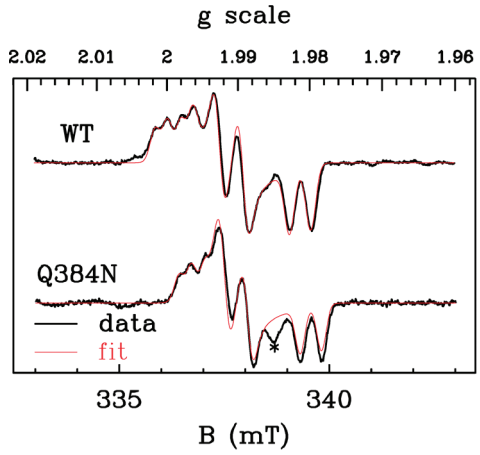

FIGURE 3: EPR signatures of the Mo(V) active site in "as-purified" WT and Q384N *Rs* NapAB. Conditions: modulation amplitude 0.1 mT, microwave power 1 mW, temperature 55 K, and microwave frequency 9.408 GHz. The red lines show the simulations performed by using the EasySpin free package (*29*) with the following parameters: WT, g = 1.9989, 1.9908, 1.9812, hyperfine couplings with protons A_1 = 0.61, 0.56, and 0.50 mT, A_2 = 0.29, 0, and 0 mT, g-strain parameters for line broadening σ = 0.0016, 0.0016, and 0.0016; Q384N, g = 1.9955, 1.9901, and 1.9797, A_1 = 0.61, 0.53, and 0.50 mT, A_2 = 0.29, 0, and 0 mT, σ = 0.0016, 0.0016, and 0.0015. We assumed that the principal axes of the A and g tensors are parallel. The additional line at g = 1.985 (marked by an asterisk) may result from the noncollinearity of the tensors (*30*, *31*).

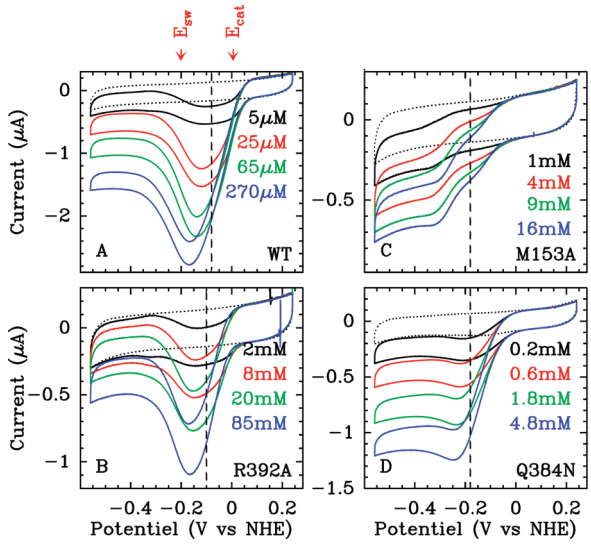

FIGURE 4: Steady-state voltammetry of WT *Rs* NapAB (panel A) and three mutants, R392A (panel B), M153A (panel C), and Q384N (panel D), adsorbed at a rotating graphite disk electrode, at pH 7.7, 25 °C, scan rate ν = 20 mV/s, and electrode rotation rate 4 krpm. The nitrate concentrations are indicated in each panel. The vertical dashed lines mark the reduction potentials of the [4Fe4S] cluster, determined in potentiometric titrations followed by EPR. The red arrows above panel A mark the values of the parameters E_{cat} and E_{sw} for the WT enzyme at 25 mM nitrate.

as the other features of the signal, and it is likely to arise from noncollinearity effects of the g and hyperfine tensors (*30*, *31*). This feature can also be observed as a shoulder at g = 1.986 in the high-g signal of the WT enzyme. This suggests that the mutation induced very small structural changes leading to only small variations of the Mo(V) g-values and hyperfine tensor orientations. In reductive titrations followed by EPR the high-g signal of Q384N disappears at −105 mV at pH 7.5, and the sample becomes EPR silent. As observed with the WT enzyme (*25*), this reduction is irreversible: no signal is detected upon reoxidation of the sample either with ferricyanide or oxygen. From the similarity between the spectral signatures and the redox behaviors of the Mo(V) species observed in as-prepared WT and Q384N NapAB, we conclude that this species, which we think is not part of the catalytic cycle, is only slightly affected by the Q384N mutation.

Electrochemical Portraits of the Mutants. Figure 4 shows representative voltammetric signals obtained with each of the four enzymes discussed here, the WT form of *Rs* NapAB and the R392A, M153A, and Q384N mutants (panels A, B, C, and D, respectively). The dotted lines are blanks, recorded with the enzyme adsorbed on the electrode but in the absence of nitrate. The black, red, green, blue, and magenta lines are voltammograms recorded with increasing concentrations of nitrate, respectively, as indicated in each panel. Each nitrate concentration range was chosen according to the value of the Michaelis constants relative to nitrate, which increases in the order WT < Q384N < M153A < R392A (Table 1). All signals were recorded at pH 7.7, 25 °C. In each plot, the vertical dashed line marks the reduction potential of the [4Fe4S] cluster determined in titrations followed by EPR.

Figure 4A shows the reference voltammograms obtained with the WT enzyme (see also refs *8* and *9*). At high potential (E positive versus SHE) the enzyme is too oxidized to reduce nitrate, and the current is not different from the baseline (dotted line). The activity kicks off when the electrode potential becomes lower than about +50 mV vs SHE, irrespective of nitrate concentration. When the potential is swept toward negative values, the activity increases (the current decreases) until it reaches a maximum at $E \approx -100$ mV (the exact value depending on nitrate concentration) and then decreases and reaches a limiting value on the plateau at low potential. The reverse scan shows the same activity profile (the current is only offset by the effect of electrode charging), showing that the activity is in a steady state. The limiting and peak currents depend on nitrate concentration. Catalytic currents cannot be converted into turnover numbers since the amount of enzyme adsorbed on the electrode is unknown, but from the change in limiting current against nitrate concentration, a Michaelis constant of about 80 μM can be estimated, in agreement with the results in ref *34* (95 μM at pH 7, E = −510 mV, 25 °C).

If one examines the dependence of current on nitrate concentration at a given potential, the data in Figure 4A show that the current levels off at a lower concentration when the electrode potential is greater; this decrease of K_m upon increasing E is one of the predictions of the kinetic model in refs *8* and *9*, which assumes that the rate of substrate binding depends on the redox state of the Moco and is smaller when the Mo is fully reduced. The values of K_m determined from the electrochemical measurement are all lower than that estimated in solution assays with reduced MV as the electron donor: 400 μM at pH 8, 30 °C, in Table 1. Regarding *P. pantotrophus* NapAB, the Michaelis constant determined in PFV also decreases when the potential increases, and even the greatest value is lower than that measured in solution assays (*10*). This demonstrates that the Michaelis constant of NapAB is not a pure dissociation constant, consistent with the model in refs *8* and *9* and the observation in ref *22* that the values of V_m and K_m determined in solution assays are different for NapA and NapAB.

The shape of these complex voltammograms is often characterized by the phenomenological parameters called E_{cat} and

E_{sw}, the "catalytic" and "switch" potentials, defined as the positions of maximum slope on either side of the peak in the $i(E)$ profile (*13*, *19*), as indicated by arrows above Figure 4A. Regarding the WT enzyme, we showed that the high potential flank of the signal has a complex underlying structure at high concentration of nitrate (Figure 11 in ref *9*), and the value of E_{cat} is therefore only a crude characterization of the position of the wave. Additionally, we note that E_{sw} decreases as the concentration of nitrate increases (Figure 4A) and that it is always more than 100 mV lower than the value of the reduction potential of the [4Fe4S] cluster, indicated by a vertical dashed line.

The voltammograms of the R392A mutant are shown in Figure 4B. In agreement with the finding in solution assays that the mutation greatly increases the Michaelis constant (Table 1 and ref *23*), Figure 4B shows that the enzyme is not saturated at a nitrate concentration of 20 mM (green line). Compared to the WT enzyme, the onset of activity is shifted about 50 mV down, but the waveform is essentially similar, with a pronounced decrease in activity at low potential. Again, the value of the reduction potential of the [4Fe4S] cluster (vertical dashed line) does not match the value of E_{sw}.

Regarding the M153A variant (Figure 4C), the change in current against nitrate concentration suggests that the Michaelis constant is in the millimolar range, consistent with the value determined in solution assays with MV. The mutation has a strong effect on this waveform, which exhibits a high potential shoulder at about −100 mV and a further "boost" of activity around −250 mV. The decrease in activity at low potential is very weak or even absent, depending on nitrate concentration.

In Figure 4D, the voltammograms of the Q384N mutant also suggest that its K_m is in the millimolar range, and this is in agreement with the results in Table 1. Again, the mutation significantly affects the wave shape: at 0.6 mM nitrate, for example (red line), the decrease in activity at low potential is less pronounced than for the WT and R392A enzymes, and this low-potential feature nearly disappears at a higher concentration of nitrate (see, e.g., the blue line at 4.8 mM nitrate).

Solution Assays. In the past, solution assays were carried out on the bench using a sealed optical cuvette flushed with argon. However, to minimize the problems caused by oxygen leaks, we now routinely assay nitrate reductase using a small water-jacketed glass cell stirred with a rotating magnet and located in an anaerobic glovebox. We measure the absorbance (A) using a microprobe (3.05 mm diameter) connected with an optic fiber to a UV/visible spectrophotometer. The procedure consists in reducing by sodium dithionite (DT) a solution containing MV and excess nitrate and then starting the assay by adding the enzyme. In the experiment in Figure 5, the initial concentration of oxidized MV was 500 μM, and we added dithionite at $t \approx 1$, 1.5, and 2 min to give a final DT concentration of 21, 42, and 51 μM. The increase in absorbance at 604 nm (black trace in Figure 2A) is fully consistent with MV being quantitatively reduced by DT with a stoichiometry of 1DT/2MV ($\varepsilon^{604}_{MVred} = 13.6\ M^{-1}\ cm^{-1}$). This results in the following concentrations of reactants: [reduced DT] = 0, [MVred] ≈ 100 μM, [MVox] ≈ 400 μM, and nitrate 20 mM. The reaction was then started at $t = 3$ min by adding an aliquot of stock solution of enzyme.

The red trace and the right Y axis in Figure 5A show the instant rate of MV oxidation ($-dA/dt$) plotted against time. The rate increases about 2-fold over the course of the assay, as reduced MV is consumed, and the reaction ultimately stops when MV is completely exhausted (nitrate is in large excess over MV).

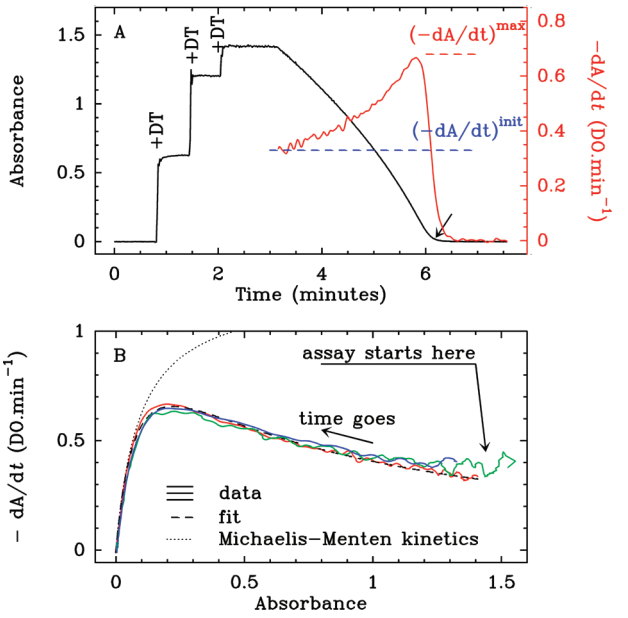

FIGURE 5: Solution assay of WT *Rs* NapAB. Panel A shows the change in absorbance against time (blue trace); the enzyme (final concentration ≈4 nM from a stock solution ≈2 μM) is added at $t = 3$ min. The red line in panel A shows the rate of MV oxidation ($-dA/dt$) obtained by differentiating the $A(t)$ signal. In panel B, the results of three independent experiments (blue, green, and red, solid traces) are plotted as absorbance change against absorbance and fitted to eq 1. The dotted line illustrates the Michaelien behavior. Experimental conditions: pH 7.5, $T = 25$ °C, $[NO_3^-] = 20$ mM. The green, red, and blue solid traces correspond to slightly different amounts of DT (from ~45 to 55 μM), concentrations of MV (red, 0.5 mM; green and blue, 5 mM), and concentrations of enzyme (4, 3, and 6 nM for the red, green, and blue, respectively; the values of $-dA/dt$ were normalized to match the data obtained with a final concentration of 4 nM).

Figure 5B shows the change of $-dA/dt$ against A. This is nothing but the change of rate of MVred consumption against MVred concentration. We plotted three independent data sets (blue, black, and red lines), obtained from experiments with various concentrations of enzyme, total MV, and added dithionite. The three traces start at a difference value of the absorbance, because the initial concentration of MVred is different, but as time goes, the three traces overlay, which demonstrates that the observed rate depends only on the instant concentration of MVred. The rate is lower when the concentration of reduced MV is large (under very reducing conditions). The deviation from the normal Michaelis−Menten behavior, indicated by a dotted line, is very clear.

The data can be fit to

$$-dA/dt = \frac{v_1}{1 + K_1/A + A/K_2} \qquad (1)$$

by adjusting v_1, K_1, and K_2. This equation, which was used in ref *21* to fit the results of the spectrophotometric assay of periplasmic DMSO reductase, can be derived from a model that assumes linear inhibition by excess MVred (*35*). K_1 corresponds to the Michaelis constant, and K_2 is an inhibition constant. However, for reasons that will be clear later, we prefer to consider this equation as purely empirical, and we do not emphasize here the physical meanings of the parameters. When A tends to 0, just before complete exhaustion of MVred, $-dA/dt$ is proportional to A, which results in an exponential

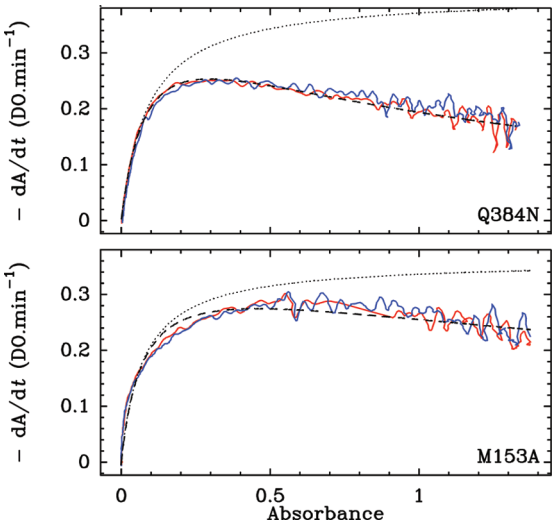

FIGURE 6: Time course of the assay of the Q384 (top panel) and M153A (bottom panel) variants. Experimental conditions: T = 25 °C, pH = 7.5, [NO_3^-] = 20 mM. In each panel, the red and blue traces correspond respectively to a total MV concentration of 0.5 and 5 mM, respectively. The data are fitted by eq 1 (dashed lines). The best values of K_1 and K_2 were 6 and 73 μM MVred for Q384N and 5 and 200 μM MVred for M153A. The dotted lines illustrate the Michaelien behavior.

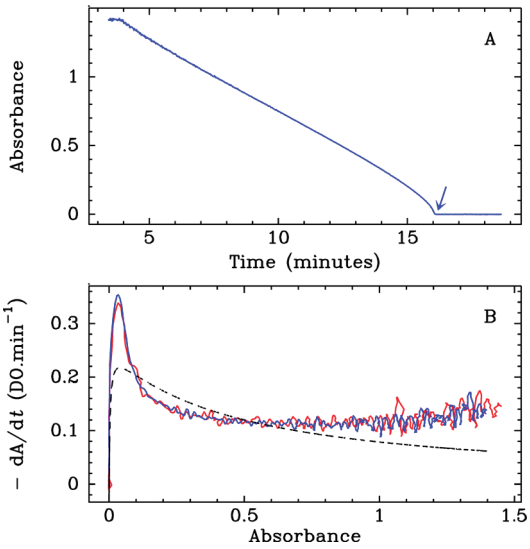

FIGURE 7: The time course of the solution assay of the R392A variant. Panel A: Absorbance (A) against time. Panel B: Change in absorbance against absorbance. In panel B, two data sets are overlaid (they differ by their total concentration of MV: 0.5 and 5 mM for the red and blue traces, respectively; other experimental conditions are T = 25 °C, pH = 7.5, and [NO_3^-] = 100 mM. The dotted line is the (unsuccessful) fit to eq 1.

decrease of the absorbance (pointed to by an arrow in Figure 5A) with a time constant τ given by

$$\tau = K_1/v_1 \qquad (2)$$

Equation 1 describes well the entire data in Figure 5 (dashed lines), and the fit returned v_1 = 1.2 min^{-1}, K_1 = 0.09, and K_2 = 0.5 absorbance units (K_1 = 7 μM and K_2 = 40 μM MVred, respectively).

Figure 6 shows the data obtained with the Q384N and M153A mutants. The $A(t)$ traces (not shown) have the same shape as for the WT enzyme, and the plots of $-dA/dt$ against A could also be fitted to eq 1 (dashed lines in Figure 6).

Figure 7 shows a typical result obtained with the R392A mutant. Although the trace in Figure 7A is mostly linear, an acceleration is clearly visible at t = 16 min, just before exhaustion of MVred. That the reaction stops in a very abrupt maner (arrow in Figure 7A) shows that the value of K_1 in eq 1 is extremely small (cf. eq 2). The dotted line is the best fit to eq 1: clearly, the inhibition model that is used to derive eq 1 does not apply in this case. This is because eq 1 predicts that the activity should drop to zero when A is above K_2, whereas the data in Figure 7B show that the activity tends to a plateau under very reducing conditions. This may actually also be true in the case of the three other enzymes, but the deviation from eq 1 will escape detection unless K_1 and K_2 are so small that the concentration of MVred is saturating when the assay starts (as occurs for the R392A variant).

Correlation between the Results of PFV and Solution Assays. Figure 8 is an attempt to compare the profiles of activity against potential observed in solution assays and protein film voltammetry (Figure 4). We display again the solution data shown in Figures 5B (WT enzyme), 6, and 7 (mutants) using plots of rate ($-dA/dt$) against "solution potential".[2] The latter was calculated from the Nernst equation, the reduction potential of MV (E^0_{MV} = −440 mV), the total concentration of MV ([MVtot]), and the *instant* concentration of reduced MV ([MVred](t) = $A(t)/\epsilon_{MV}l$) according to

$$E(t) = E^0_{MV} + \frac{RT}{F}\ln\left(\frac{[\mathrm{MVtot}] - [\mathrm{MVred}](t)}{[\mathrm{MVred}](\mathrm{t})}\right) \qquad (3)$$

The spectrophotometric data obtained with a total concentration of MV of 0.5 mM (red traces) or 5 mM (blue and green traces) are superposed in the plots of dA/dt against A (Figures 5, 6, and 7) but not in the plots dA/dt against E (Figure 8); this shows that the activity is uniquely defined by [MVred], not by the ratio [MVox]/[MVred].

However, we found a relation between the magnitude of the low-potential attenuation of activity in PFV and the deviation from Michaelien behavior in solution assays: for example, the switch is nearly absent from the electrochemical signature of the M153A variant in Figure 4C, and the plot in Figure 6 shows that there is little increase in activity over the course of the solution assay. In contrast, both phenomena are very pronounced in the case of the R392A variant (Figures 4B and 7).

To make this correlation semiquantitative, we plotted in Figure 9 the ratios of maximal rate over initial rates in solution assays (the parameters defined in Figure 5A) against the ratios i_{peak}/i_{lim} determined from the voltammograms recorded at a high concentration of substrate (as defined in Figure 1A). The large error bars result from the fact that the ratio i_{peak}/i_{lim} depends on nitrate concentration (*9*): we used the data obtained with the two largest concentrations in each panel of Figure 4 to calculate the average i_{peak}/i_{lim} and the error. The data points in Figure 9 fall surprisingly close to the line $y = x$, which strongly supports the view that the voltammetric peaks in Figure 4 and the acceleration in solution assays actually reveal the same phenomenon.

Last, we note that we observed no striking correlation between the ratio of peak over limiting currents defined in Figure 1A and the value of E_{sw}. The latter is not significantly affected by the R292A mutation, and it is undefined regarding M153A.

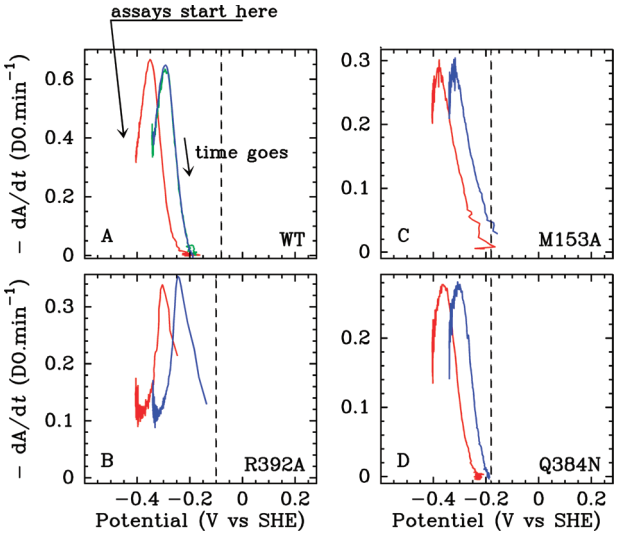

FIGURE 8: Rates ($-dA/dt$) plotted against "solution potential",[2] calculated from the instant concentrations of oxidized and reduced MV and the Nernst equation (eq 3). The data are those plotted in Figures 5A for the WT (panel A), 7B for the R392A variant (panel B), and 6 for the M153 and Q384N variants (panels C and D, respectively). The color code is also respected: the data obtained with a concentration of oxidized MV (before DT is added) of 5 mM are plotted as green and blue traces, while the red trace is for 0.5 mM MV. Nitrate concentration: 20 mM for WT and M153A and Q384N variants and 100 mM for the R392A mutant. T = 25 °C. As in Figure 4, the vertical dashed lines mark the reduction potential of the [4Fe4S] cluster, determined in potentiometric titrations.

DISCUSSION

The absorbance of reduced MV is so high that it cannot be used in great excess over the physiological substrate (nitrate, DMSO) in solution assays. Therefore, the thermodynamic driving force provided by the reduced viologen changes (although only slightly) over the course of the experiment. The experiments in Figures 1B and 5−7 are in line with the earlier observations that the turnover rates of periplasmic *R. capsulatus* DMSO reductase and *P. pantotrophus* nitrate reductase progressively increase as the viologen radical is oxidized (*21*, *10*). Several explanations have been put forward, none of which gives eq 1 justification.

(1) Bray and co-workers have envisaged that the acceleration could result from the exhaustion of the DT that is initially in excess (*21*). They ruled this out, because this does not explain their observation that the effect is more pronounced with benzyl viologen than with MV. In our experiments, we made sure that the reduction of MV by DT is quantitative (cf. the above description of the blue trace in Figure 5), and therefore we also consider this hypothesis as unlikely.

(2) Another suggestion in ref *21* was that the effect may be a consequence of the dimerization of the radicals at high concentration. This hypothesis does not explain that the phenomenon is enzyme dependent: acceleration is not seen in the assays of, e.g., fumarate reduction by *E. coli* fumarate reductase (*36*) or of hydrogen production by NiFe hydrogenase (*4*). Moreover, we have shown that the behavior in solution assays is also affected by the mutation of amino acids that are close to the active site (compare Figures 6 and 7).

(3) Another proposal was that the inhibition by high concentrations of reduced viologen results from the overreduction of the enzyme molecule by the viologen (*21*). In this respect, it is remarkable that the PFV experiments also show that very

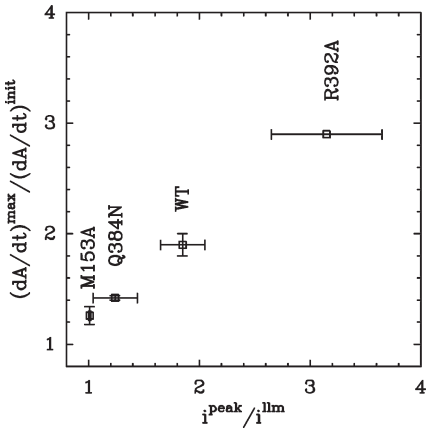

FIGURE 9: Correlation between the ratio of the maximal over initial rates in solution assays and the ratio i_{peak}/i_{lim} determined from the voltammograms in Figure 4. These parameters are defined in Figure 1.

reducing conditions make the activity decrease (see, e.g., Figure 1A) (*19*, *10*).[4] We could rule out the possibility that this is a coincidence by observing in Figure 9 a very clear correlation between the magnitude of the switch in PFV (the ratio of peak over limiting currents defined in Figure 1A) and the magnitude of the acceleration in solution assays (the ratio of maximal over initial rates, defined in Figure 1B). This is unambiguous evidence that the two phenomena have the same origin. Electrochemical measurements, which demonstrate the existence of an optimal potential window for catalysis by the enzymes of the DMSO reductase family (Figure 1A), therefore support the suggestion that overreduction partly inactivates the enzyme, although the exact mechanism by which this occurs is debated.

Bray suggested that this may result from the loss of an oxygen ligand from the metal or the reduction of a pterin to the tetrahydro state (*21*), but more recent experiments by Hille and co-workers showed that the two pterins of periplasmic DMSO reductase are not redox active (*37*). We note that the "overreduction" must be reversible for the activity to increase over time. Butt and co-workers proposed that the reduction that inactivates NapAB is that of the [4Fe4S] cluster that is closed to the Mo (*10*). However, we observed no simple correlation between the position of the different features of the catalytic wave and the reduction potential of the [4Fe4S] cluster (indicated by the vertical dashed lines in Figure 4). For example, in WT and R392A *Rs* NapAB, the switch potential does not coincide with the reduction potential of the cluster (unlike in WT *P. pantotrophus* NapAB (*10*)), and if we compare the data obtained with WT and Q384N *Rs* NapAB at low concentration of nitrate (black lines), the position of E_{sw} seems not to be affected by the −100 mV shift in reduction potential of the cluster. Overall, this seems conclusive regarding the fact that the attenuation of activity at low electrode potential is not caused by the [4Fe4S] cluster acting as a redox switch. Instead, since the amino acids that have been mutated here are all close to the active site Mo (Figure 2B), the fact that their substitutions greatly affect the wave shapes suggests that the latter is a signature of the active site chemistry. Since the rate of reduction of the enzyme during turnover is proportional to the concentration of MVred (see below), this suggests that the catalytic activity increases when the rate of

[4]The same correlation between the results of solution assays and PFV was observed in the case of fumarate reduction by succinate dehydrogenase (*12*, *36*).

reduction of the enzyme decreases below a certain threshold. This supports our previous interpretation of the voltammetry of the WT enzyme (*8*, *9*, *3*): catalysis can follow distinct routes, as substrate binding either precedes or follows the reduction from Mo(V) to Mo(IV), and the relative rates of the two reactions determine which track is used, the Mo(V) state acting as a railway switch. We have previously emphasized the correlation between the position of E_{sw} and the potential of reduction of the Mo(V) species that exhibits the high-*g* signature (*8*, *9*). However, since we now know that the Mo(V) signature actually corresponds to an inactive species (*25*), this correlation appears to be fortuitous.

Figure 4 shows that the mutations have a spectacular effect on the wave shapes. Overall, the electrochemical results confirm the finding that all three mutations increase the Michaelis constants, the stronger effect being caused by the R392A mutation. Most interestingly, we observed that all mutations increase the overpotential for nitrate reduction (they shift the catalytic signal toward higher driving force). The electrochemical signals of the mutants are not broader than that of the WT; they remain sharp and well-defined, which suggests that the shift toward low potential does not result from interfacial electron transfer limitations (*3*, *38*). This is consistent with the fact that modifying amino acids that are buried within the enzyme is unlikely to affect the rate of interfacial electron transfer (see, however, ref *39*). Catalysis by nitrate reductase requires a significant driving force even in the WT enzyme: the onset of catalysis appears at a much lower potential than the reduction potential of the nitrate/nitrite couple (+430 mV at pH 7 (*40*)); this is in contrast with NiFe and FeFe hydrogenases, for example, for which fast turnover is obtained with very little overpotential (*41*, *42*). The fact that the mutations increase further (by about 50 mV) the driving force required to elicit catalysis is interesting evidence that they decrease the efficiency of the catalyst. Considering the efforts spent in analyzing the wave shapes for the WT enzyme (*9*), the quantitative analysis of the data in Figure 4 is a formidable challenge which is out of the scope of this paper.

We now discuss the relation between the experimental parameters that determine the "driving force" in solution assays and PFV experiments.

Our results in Figures 5B, 6, and 7 demonstrate that the rate of nitrate reduction is independent of the concentration of *oxidized* MV. This implies that, in this case, the "solution potential"[2] calculated from the reduction potential of the MV and the ratio [MVox]/[MVred] (eq 3) is not a relevant parameter. Indeed, the activity profiles in Figure 8 do not superimpose when they are plotted as a function of this "solution potential". This observation contrasts with the findings of Fernandez et al., who showed that the *steady-state* rate of hydrogen production by NiFe hydrogenase increases in a sigmoidal manner as the "solution potential" is decreased (*4*).

The thermodynamic driving force of a reaction is the Gibbs energy change, ΔG, calculated from the standard Gibbs energy change for the reaction and the concentrations of reactants and products. In the present case, the standard Gibbs energy change is extremely negative because the difference between the standard reduction potentials of the nitrate/nitrite and MVox/MVred couples is greater than 800 mV, and the reaction continuously evolves in the direction of reduction of nitrate by MVred.

From the point of view of kinetics, our data show that what matters most is the reversibility of the reaction between the enzyme and the electron donor. The rate of electron transfer from MV to the enzyme depends, according to Marcus theory, on the difference between the standard reduction potentials of the surface-exposed heme and MV. That this difference is very large (of the order of +300 mV) makes ET to the enzyme irreversible. Therefore, the rate of nitrate reduction by NapAB should depend only on the concentration of reactants. This is actually exactly what Figures 5B, 6, and 7 show: the rate depends only on [MVred] (the concentration of nitrate is constant in these experiments). The fact that this dependence is complex is an intrinsic property of the catalyst.

In contrast, when NapAB is adsorbed onto an electrode, the shape of the voltammograms is well described by assuming that the redox state of the active site is related to the electrode potential by the Nernst equation (*8*, *9*). This is unambiguous evidence that in electrochemistry experiments interfacial electron transfer to and from the enzyme, in either direction, is much faster than turnover (*38*).

Regarding the experiments with NiFe hydrogenase in ref *4*, [MVred] was maintained constant (1 mM) and saturating. The enzyme reversibly catalyzes the conversion between H^+ and H_2 (*43*), and the reduction potential of the surface-exposed [4Fe4S] cluster in hydrogenase is close to that of MV (*44*). Electron transfer to and from the enzyme is reversible, and this equilibrium is dictated by the Nernst equation. This is the reason there is a relation (although it is complex) between rate and "solution potential" in this case.

This shows that the electrode potential, or the "solution potential"[2] calculated from the concentrations of the oxidized and reduced redox partner (eq 3), determines the rate of the reactions when electron transfers to and from the enzyme are faster than turnover (according to the electrochemical terminology, this is the "reversible" limit). In contrast, when electron transfer to or from the enzyme is irreversible, the rate in solution assays depends on the concentration of *reactants*; the fact that the concentration of products is irrelevant implies that there can be no relation in that case between *kinetics* and Gibbs energy change.

REFERENCES

1. Léger, C., Elliott, S. J., Hoke, K. R., Jeuken, L. J. C., Jones, A. K., and Armstrong, F. A. (2003) Enzyme electrokinetics: using protein film voltammetry to investigate redox enzymes and their mechanisms. *Biochemistry 42*, 8653–8662. DOI: 10.1021/bi034789c.
2. Armstrong, F. (2009) Dynamic electrochemical experiments on hydrogenases. *Photosynth. Res. 102*, 541–550. DOI: 10.1007/s11120-009-9428-0.
3. Léger, C., and Bertrand, P. (2008) Direct electrochemistry of redox enzymes as a tool for mechanistic studies. *Chem. Rev. 108*, 2379–2438. DOI: 10.1021/cr0680742.
4. Fernandez, V., Aquirre, R., and Hatchikian, E. (1984) Reductive activation and redox properties of hydrogenase from *Desulfovibrio gigas*. *Biochim. Biophys. Acta 790*, 1–7. DOI: 10.1016/0167-4838(84)90324-8.
5. Elliott, S. J., Léger, C., Pershad, H. R., Hirst, J., Heffron, K., Blasco, F., Rothery, R., Weiner, J., and Armstrong, F. A. (2002) Detection and interpretation of redox potential optima in the catalytic activity of enzymes. *Biochim. Biophys. Acta 1555*, 54–59. DOI: 10.1016/S0005-2728(02)00254-2.
6. Hille, R. (2002) Molybdenum and tungsten in biology. *Trends Biochem. Sci. 27*, 360–367. DOI: 10.1016/S0968-0004(02)02107-2.
7. Moura, J. J., Brondino, C. D., Trincao, J., and Romao, M. J. (2004) Mo and W bis-MGD enzymes: nitrate reductases and formate dehydrogenases. *J. Biol. Inorg. Chem. 9*, 791–799. DOI: 10.1007/s00775-004-0573-9.
8. Frangioni, B., Arnoux, P., Sabaty, M., Pignol, D., Bertrand, P., Guigliarelli, B., and Léger, C. (2004) *Rhodobacter sphaeroides* respiratory nitrate reductase, the kinetics of substrate binding favors intramolecular electron transfer. *J. Am. Chem. Soc. 126*, 1328–1329. DOI: 10.1021/ja0384072.

9. Bertrand, P., Frangioni, B., Dementin, S., Sabaty, M., Arnoux, P., Guigliarelli, B., Pignol, D., and Léger, C. (2007) Effects of slow substrate binding and release in redox enzymes: Theory and application to periplasmic nitrate reductase. *J. Phys. Chem. B 111*, 10300–10311. DOI: 10.1021/jp074340j.
10. Gates, A. J., Richardson, D. J., and Butt, J. N. (2008) Voltammetric characterisation of the aerobic energy dissipating nitrate reductase of *Paracoccus pantotrophus*: exploring the activity of a redox balancing enzyme as a function of electrochemical potential. *Biochem. J. 409*, 159–168. DOI: 10.1042/BJ20071088.
11. Pershad, H. R., Hirst, J., Cochran, B., Ackrell, B. A. C., and Armstrong, F. A. (1999) Voltammetric studies of bidirectional catalytic electron transport in *Escherichia coli* dehydrogenase: comparison with the enzyme from beef heart mitochondria. *Biochim. Biophys. Acta 1412*, 262–272. DOI: 10.1016/S0005-2728(99)00066-3.
12. Sucheta, A., Ackrell, B. A. C., Cochran, B., and Armstrong, F. A. (1992) Diode-like behaviour of a mitochondrial electron-transport enzyme. *Nature 356*, 361–362. DOI: 10.1038/356361a0.
13. Hirst, J., Sucheta, A., Ackrell, B. A. C., and Armstrong, F. A. (1996) Electrocatalytic voltammetry of succinate dehydrogenase: direct quantification of the catalytic properties of a complex electron-transport enzyme. *J. Am. Chem. Soc. 118*, 5031–5038. DOI: 10.1021/ja9534361.
14. Hirst, J., Ackrell, B. A. C., and Armstrong, F. A. (1997) Global observation of hydrogen/deuterium isotope effect on bidirectional catalytic electron transport in an enzyme: direct measurement by protein-film voltammetry. *J. Am. Chem. Soc. 119*, 7434–7439. DOI: 10.1021/ja9631413.
15. Barker, C. D., Reda, T., and Hirst, J. (2007) The flavoprotein subcomplex of complex I (NADH:ubiquinone oxidoreductase) from bovine heart mitochondria: insights into the mechanisms of NADH oxidation and NAD^+ reduction from protein film voltammetry. *Biochemistry 46*, 3454–3464. DOI: 10.1021/bi061988y.
16. Angove, H. C., Cole, J. A., Richardson, D. J., and Butt, J. N. (2002) Protein film voltammetry reveals distinctive fingerprints of nitrite and hydroxylamine reduction by a cytochrome *c* nitrite reductase. *J. Biol. Chem. 277*, 23374–23381. DOI: 10.1074/jbc.M200495200.
17. Almeida, M. G., Guigliarelli, B., Bertrand, P., Moura, J. J. G., Moura, I., and Léger, C. (2007) A needle in a haystack: the active site of the membrane-bound complex cytochrome *c* nitrite reductase. *FEBS Lett. 581*, 284–288. DOI: 10.1016/j.febslet.2006.12.023.
18. Rapson, T. D., Kappler, U., and Bernhardt, P. V. (2008) Direct catalytic electrochemistry of sulfite dehydrogenase: mechanistic insights and contrasts with related Mo enzymes. *Biochim. Biophys. Acta 1777*, 1319–1325. DOI: 10.1016/j.bbabio.2008.06.005.
19. Heffron, K., Léger, C., Rothery, R. A., Weiner, J. H., and Armstrong, F. A. (2001) Determination of an optimal potential window for catalysis by *Escherichia coli* dimethyl sulfoxide reductase, and hypothesis on the role of Mo^V in the reaction pathway. *Biochemistry 40*, 3117–3126. DOI: 10.1021/bi002452u.
20. Elliott, S. J., Hoke, K. R., Heffron, K., Palak, M., Rothery, R. A., Weiner, J. H., and Armstrong, F. A. (2004) Voltammetric studies of the catalytic mechanism of the respiratory nitrate reductase from *Escherichia coli*: how nitrate reduction and inhibition depend on the oxidation state of the active site. *Biochemistry 43*, 799–807. DOI: 10.1021/bi035869j.
21. Adams, B., Smith, A., Bailey, S., McEwan, A., and Bray, R. (1999) Reactions of dimethylsulfoxide reductase from *Rhodobacter capsulatus* with dimethyl sulfide and with dimethyl sulfoxide: complexities revealed by conventional and stopped-flow spectrophotometry. *Biochemistry 38*, 8501–8511. DOI: 10.1021/bi9902034.
22. Arnoux, P., Sabaty, M., Alric, J., Frangioni, B., Guigliarelli, B., Adriano, J. M., and Pignol, D. (2003) Structural and redox plasticity in the heterodimeric periplasmic nitrate reductase. *Nat. Struct. Mol. Biol. 10*, 928–934. DOI: 10.1038/nsb994.
23. Dementin, S., Arnoux, P., Frangioni, B., Grosse, S., Léger, C., Burlat, B., Guigliarelli, B., Sabaty, M., and Pignol, D. (2007) Access to the active site of periplasmic nitrate reductase: insights from site-directed mutagenesis and zinc inhibition studies. *Biochemistry 46*, 9713–9721. DOI: 10.1021/bi700928m.
24. Liebgott, P.-P., Leroux, F., Burlat, B. A. A., Dementin, S. A., Baffert, C., Lautier, T., Fourmond, V., Ceccaldi, P., Cavazza, C., Meynial-Salles, I., Soucaille, P., Fontecilla-Camps, J. C., Guigliarelli, B., Bertrand, P., Rousset, M., and Léger, C. (2010) Relating diffusion along the substrate tunnel and oxygen sensitivity in hydrogenase. *Nat. Chem. Biol. 6*, 63–70. DOI: 10.1038/nchembio.276.
25. Fourmond, V., Burlat, B., Dementin, S., Arnoux, P., Sabaty, M., Boiry, S., Guigliarelli, B., Bertrand, P., Pignol, D., and Léger, C. (2008) Major Mo(V) EPR signature of *Rhodobacter sphaeroides* periplasmic nitrate reductase arising from a dead-end species that activates upon reduction. relation to other molybdoenzymes from the DMSO reductase family. *J. Phys. Chem. B 112*, 15478–15486. DOI: 10.1021/jp807092y.
26. Fourmond, V., Hoke, K., Heering, H. A., Baffert, C., Leroux, F., Bertrand, P., and Léger, C. (2009) Soas: a free software to analyse electrochemical data and other one-dimensional signals. *Bioelectrochemistry 76*, 141–147. DOI: 10.1016/j.bioelechem.2009.02.010.
27. Roldan, M. D., Sears, H. J., Cheesman, M. R., Ferguson, S. J., Thomson, A. J., Berks, B. C., and Richardson, D. J. (1998) Spectroscopic characterization of a novel multihemec-type cytochrome widely implicated in bacterial electron transport. *J. Biol. Chem. 273*, 28785–28790. DOI: 10.1074/jbc.273.44.28785.
28. Sabaty, M., Avazeri, C., Pignol, D., and Vermeglio, A. (2001) Characterization of the reduction of selenate and tellurite by nitrate reductases. *Appl. Environ. Microbiol. 67*, 5122–5126. DOI: 10.1128/AEM.67.11.5122-5126.2001.
29. Stoll, S., and Schweiger, A. (2006) Easyspin, a comprehensive software package for spectral simulation and analysis in EPR. *J. Magn. Reson. 178*, 42–55. DOI: 10.1016/j.jmr.2005.08.013.
30. Golding, R. M., and Tennant, W. C. (1973) A study of the effect of non-collinear zeeman, hyperfine and fine structure tensors on E.S.R. spectra. *Mol. Phys. 25*, 1163–1171. DOI: 10.1080/00268977300101001.
31. Mabbs, F. , and Collison, D. (1992) Electron Paramagnetic Resonance of d Transition Metal Compounds, Elsevier Science, Amsterdam.
32. Bennett, B., Berks, B. C., Ferguson, S. J., Thomson, A. J., and Richardson, D. J. (1994) Mo(V) electron paramagnetic resonance signals from the periplasmic nitrate reductase of *Thiosphaera pantotropha*. *Eur. J. Biochem. 226*, 789–798. DOI: 10.1111/j.1432-1033.1994.00789.x.
33. Fourmond, V., Sabaty, M., Arnoux, P., Bertrand, P., Pignol, D., and Léger, C. (2010) Reassessing the strategies for trapping catalytic intermediates during nitrate reductase turnover. J. Phys. Chem. B (in press). DOI: 10.1021/jp911443y.
34. Fourmond, V., Lautier, T., Baffert, C., Leroux, F., Liebgott, P.-P., Dementin, S., Rousset, M., Arnoux, P., Pignol, D., Meynial-Salles, I., Soucaille, P., Bertrand, P., and Léger, C. (2009) Correcting for electrocatalyst desorption and inactivation in chronoamperometry experiments. *Anal. Chem. 81*, 2962–2968. DOI: 10.1021/ac8025702.
35. Cornish-Bowden, A. (2004) Fundamental of Enzyme Kinetics, Portland Press, Colchester, U.K.
36. Ackrell, B. A. C., Armstrong, F. A., Cochran, B., Sucheta, A., and Yu, T. (1993) Classification of fumarate reductase and succinate dehydrogenases based upon their contrasting behaviour in the reduced benzylviologen/fumarate assay. *FEBS Lett. 326*, 92–94. DOI: 10.1016/0014-5793(93)81768-U.
37. Cobb, N., Conrads, T., and Hille, R. (2005) Mechanistic studies of *Rhodobacter sphaeroides* DMSO reductase. *J. Biol. Chem. 280*, 11007–11017. DOI: 10.1074/jbc.M412050200.
38. Léger, C., Jones, A. K., Roseboom, W., Albracht, S. P. J., and Armstrong, F. A. (2002) Enzyme electrokinetics: hydrogen evolution and oxidation by *Allochromatium vinosum* [NiFe]-hydrogenase. *Biochemistry 41*, 15736–15746. DOI: 10.1021/bi026586e.
39. Léger, C., Lederer, F., Guigliarelli, B., and Bertrand, P. (2006) Electron flow in multicenter enzymes: theory, applications and consequences on the natural design of redox chains. *J. Am. Chem. Soc. 128*, 180–187. DOI: 10.1021/ja055275z.
40. Madigan, M. T., Martinko, J., and Parker, J. (2002) Brock Biology of Microorganisms, Prentice Hall, Upper Saddle River, NJ.
41. Pershad, H. R., Duff, J. L. C., Heering, H. A., Duin, E. C., Albracht, S. P. J., and Armstrong, F. A. (1999) Catalytic electron transport in *Chromatium vinosum* [Ni-Fe] hydrogenase: application of voltammetry in detecting redox-active centers and establishing that hydrogen oxidation is very fast even at potentials close to the reversible H^+/H_2 value. *Biochemistry 38*, 8992–8999. DOI: 10.1021/bi990108v.
42. Baffert, C., Demuez, M., Cournac, L., Burlat, B., Guigliarelli, B., Soucaille, P., Bertrand, P., Girbal, L., and Léger, C. (2008) Hydrogen-activating enzymes: activity does not correlate with oxygen-sensitivity. *Angew. Chem., Int. Ed. 47*, 2052–2055. DOI: 10.1002/anie.200704313.
43. Léger, C., Dementin, S., Bertrand, P., Rousset, M., and Guigliarelli, B. (2004) Inhibition and aerobic inactivation kinetics of *Desulfovibrio fructosovorans* NiFe hydrogenases studied by protein film voltammetry. *J. Am. Chem. Soc. 126*, 12162–12172. DOI: 10.1021/ja046548d.
44. Dementin, S., Belle, V., Bertrand, P., Guigliarelli, B., Adryanczyk-Perrier, G., Delacey, A., Fernandez, V. M., Rousset, M., and Léger., C. (2006) Changing the ligation of the distal [4Fe4S] cluster in NiFe hydrogenase impairs inter- and intramolecular electron transfers. *J. Am. Chem. Soc. 128*, 5209–5218. DOI: 10.1021/ja060233b.